Nuclear Instruments and Methods in Physics Research B 310 (2013) 32–36

Contents lists available at SciVerse ScienceDirect

Nuclear Instruments and Methods in Physics Research B

journal homepage: www.elsevier.com/locate/nimb

Electrical conductivity of gold-implanted alumina nanocomposite

M.C. Salvadori [a,*], F.S. Teixeira [a], L.G. Sgubin [a], M. Cattani [a], I.G. Brown [b]

[a] Institute of Physics, University of São Paulo, C.P. 66318, CEP 05314-970, São Paulo S.P., Brazil
[b] Lawrence Berkeley National Laboratory, Berkeley, CA 94720, USA

ARTICLE INFO

Article history:
Received 3 May 2013
Received in revised form 27 May 2013
Available online 6 June 2013

Keywords:
Conducting ceramic
Metal ion implantation
Surface conductivity
Percolation

ABSTRACT

We have carried out ion implantation of gold into alumina ceramic substrates and measured the surface resistivity as a function of implantation dose. The Au ion energy was 40 keV and the dose spanned the range 2.7–8.9 × 10^{16} cm^{-2}. Imaging of the implanted material by transmission electron microscopy revealed that the implanted gold self-assembles into nanoparticles, thus forming a gold-alumina nanocomposite. The surface resistivity measurements were compared with the predictions of a model based on percolation theory, in which electron transport through the composite is explained by conduction through a random resistor network formed by the Au nanoparticles. The electrical conductivity of a composite, near the critical conductor–insulator transition, is given by $\sigma \approx \sigma_0(x-x_c)^t$, where σ_0 is the saturation conductivity for which the material still remains a composite, x is the normalized metal atom concentration of the conducting phase, x_c is the critical concentration, or percolation threshold and t is the critical exponent. Excellent agreement was found between the experimental results and the predictions of the theory, and the results are consistent with prior related (but more limited) work. The percolation dose was 4.4 × 10^{16} cm^{-2}, and the critical exponent obtained was $t = 1.4 \pm 0.1$. We conclude that the conductivity process is due to percolation and that the contribution from tunneling conduction is negligible.

1. Introduction

Nanocomposites formed by metal nanoparticles embedded in an insulating matrix have some interesting electrical characteristics. According to a number of theories of transport in isotropic percolating materials [1], the electrical conductivity σ of a composite, near the critical conductor–insulator transition, is given by the scaling law $\sigma \approx \sigma_0(x-x_c)^t$, where σ_0 is the saturation conductivity for which the material still remains a composite, x is the normalized metal atom concentration of the conducting phase, x_c is the critical concentration, or percolation threshold, below which the composite has the same conductivity as the insulating host material, and t is the critical exponent. For nanocomposite materials formed by metal ion implantation into an insulator, the normalized metal atom concentration x is given by the ion implantation dose ratio φ/φ_0, where φ is the implantation dose and φ_0 (the saturation dose) is the maximum dose for which the material still remains a composite; for doses greater than φ_0 ($x = \varphi/\varphi_0 > 1$), a metal film starts to be deposited on the insulator surface and the material begins to take on the characteristics of a thin metal film.

Electron transport through granular materials consisting of small conducting regions embedded in an insulating medium can occur through either of two possible processes or their combination. When the conducting elements are in geometric contact, theory predicts that the critical exponent t is less than 2 and the process is called *percolation* [1], percolation refers to the flow of current through random resistor networks. When the conducting elements are not in geometric contact, inter-particle tunneling is dominant. Both processes may contribute separate percolation and tunneling currents; then the theory [1] predicts that the critical exponent t is greater than 2 and the process is called tunneling-percolation. Importantly, note that in these critical percolation phenomena we distinguish three regimes: (1) conductor ($x > x_c$), (2) transition ($x \approx x_c$), and (3) insulator ($x < x_c$). In the conducting regime the composite behaves like a dirty metal; the resistivity is relatively low and the temperature coefficient of the resistivity is positive. A vast class of disordered conducting-insulating materials has been analyzed in the last 30 years. It has been shown [1] that the *critical parameters* t and x_c vary in the ranges $1.5 \leqslant t \leqslant 11$ and $0.05 \leqslant x_c \leqslant 0.5$. These various composites include carbon-black-polymer systems, oxide-based thick film resistors, and other metal-inorganic and metal–organic insulator composites.

The formation of granular materials is a random process, and statistics (Monte Carlo calculations) forms the basic mathematical tool used to investigate the percolation and conductance processes. However, let us consider here the resistor-network theory as developed by Kirkpatrick [2], in which an effective-medium theory

* Corresponding author. Tel.: +55 11 3091 6857; fax: +55 11 3091 6749.
E-mail address: mcsalvadori@if.usp.br (M.C. Salvadori).

0168-583X/$ - see front matter © 2013 Elsevier B.V. All rights reserved.
http://dx.doi.org/10.1016/j.nimb.2013.05.024

of conduction in mixtures is re-examined and generalized to treat resistor networks. According to Kirkpatrick the effective conductivity σ_m of the composite is given by

$$\sigma_m = [(zx/2-1)\sigma_1 + [z(1-x)/2-1]\sigma_2]/(z-2) + [\{(zx/2-1)\sigma_1 + [z(1-x)/2-1]\sigma_2\}^2 + 2(z-2)\sigma_1\sigma_2]^{1/2}(z-2), \quad (1)$$

where z is the number of bonds at each node of the network, σ_1 is the conductivity of the conducting material, σ_2 is the conductivity of the insulating material, and x is the normalized metal atom concentration as above. This expression allows one to calculate analytically the effective conductance σ_m. Surprisingly, even though based on resistor-network theory, the σ_m predictions from this equation are accurate [2,3] – they are in fair agreement with the numerical Monte Carlo calculations.

Nanocomposites of this kind are of interest from a fundamental perspective as well as for the applications which they allow. One important application is the ability to fabricate high-voltage insulators with designer-determined surface resistivity. Metal ion implantation into alumina ceramic has been used as a technique for realizing experimenter-controlled surface resistivity (also called *sheet resistance*) of the material [4–9]. Ti and Pt have been used as implant species, ion energies have been in the 50–150 keV range, and ion implantation dose in the broad range of about 10^{11}–10^{17} cm^{-2}. Components processed in this way have included high voltage accelerator columns [5–7], support rods for electrostatic focusing lenses in single-ion devices [9], as well as small, flat coupons for basic experimental investigations. In these technological applications, the aim is to bleed off surface charge accumulation; or, said differently, to grade the voltage drop along the component in a uniform and controllable way. The approach has met with considerable success. However, little theoretical understanding of the underlying physics involved has accompanied the empirical approach, successful though it is.

In prior work we have reported on our investigations of nanocomposites including Au/PMMA [10–16] (polymethylmethacrylate), Pt/PMMA [17], Ti/alumina [18], and Au/DLC [19] (diamond like carbon) systems. In the work described here we explore the Au/alumina nanocomposite material. The Au/alumina samples were formed using a novel kind of ion implantation technique, and *in situ* resistivity measurements were performed as the implantation proceeded. Computer simulation using the TRIDYN computer code [20,21] was used to estimate the depth profiles of the ion implanted gold in the alumina substrate, and transmission electron microscopy of the implanted samples was used for direct visualization of the nanoparticles formed.

2. Experimental

Samples were formed using ion implantation of gold into small alumina coupons. In prior work by us and also by others the kind of implanter used was based on a Mevva (metal vapor vacuum arc) metal ion source; this kind of system has been well described [22–25]. In the present work we used a variant of this approach which is considerably simpler and of lower cost. We believe that the work described here constitutes the first application of this new ion implantation technique. The method has recently been described in the literature by us [26]. Briefly, in this method the plasma and the ion source are maintained at ground potential whereas the final grid and the beam injection space are at high negative potential.

In the specific embodiment of the inverted ion implanter used here for gold ion implantation into alumina substrates, we made use of a repetitively-pulsed vacuum arc plasma gun to generate pulses of dense metal plasma [27–29]. We formed gold plasma using a small vacuum arc plasma gun incorporating a gold cathode, subsequently injected into a bent-solenoid (sectional torus) magnetic filter to remove macroparticles (cathode debris). This plasma facility has been described previously [30,31]. The gun was driven by an LC pulse line of impedance 1 Ω and pulse duration 100 μs, providing a current of up to several hundred amperes at a repetition rate of up to about 3 pulses per second. The plasma stream exiting the bent-solenoid filter was directed toward the entrance of an attachment housing the negatively-biased implantation chamber. The extractor voltage was 20 kV. A magnetically-suppressed Faraday cup to monitor the implantation current density is located behind the target holder, with the holder geometry such that a known beam area is allowed to enter the cup. Thus the implantation dose can be estimated with reasonable accuracy from the Faraday cup current and the known number of pulses. The metal plasma formed in the vacuum arc discharge in general contains multiply ionized species [25,32,33]. For a gold plasma the ion charge state distribution is close to Au^+:Au^{2+}:Au^{3+} = 14:75:11 (particle fraction percent) with mean charge state $Q = 2.0$; thus the mean ion beam energy (keV) is twice the extraction voltage (kV), generating in this specific case an implantation energy of 40 keV.

The resistivity measurements were performed in situ as the implantation proceeded. For this purpose, electrical contacts were formed at both ends of the alumina sample, a small coupon of size 12×12 mm^2, using silver paint. For carrying out ion implantation, we positioned the sample near the circular entrance aperture to the Faraday cup, but not completely covering it, where the implantation ion current was monitored. Thus, after a specified number of pulses of known ion current density (as measured by the Faraday cup), leading to a calculable ion implantation dose, the implantation process would be temporarily halted and the resistance of the sample measured; then the implantation would be allowed to proceed, and so on, leading to data of resistance vs. dose.

Two independent but identical experiments were carried out, measuring the surface resistivity of the gold-implanted alumina as described above. In what follows, we will refer to sample 1 and sample 2 for these two similar experiments.

The TRIDYN [20,21] computer simulation code was used to calculate the expected depth profiles of the implanted gold in alumina. This is a Monte Carlo simulation program based on the TRIM (Transport and Range of Ions in Matter) code [34]. TRIDYN takes into account compositional changes in the substrate due to two factors: previously implanted dopant atoms, and sputtering of the substrate surface. The TRIDYN program is appropriate when the substrate composition changes significantly during the implantation process, as occurs for moderate-to-high implantation dose.

Transmission electron microscopy (TEM) was performed to visualize the gold nanoparticles inside the alumina substrate. For sample preparation, an alumina plate was scratched with a diamond tip to obtain alumina powder. The powder was sifted with a mesh sieve size of 0.062 mm to remove large grains. Then the powder was deposited on a piece of lens cleaning paper, scrubbed, and the excess removed, leaving on the surface alumina particles with grain sizes small enough for observation by TEM. A TEM copper grid covered with formvar and carbon films was then moistened in deionized water and rubbed on the paper surface containing the alumina powder. The transmission electron microscope used was a Tecnai™ G2 F20. The sample thus prepared was observed before and after gold ion implantation.

3. Results and discussion

Computer simulations of the expected gold atom depth profile in the alumina substrate were carried out using the TRIDYN program [20,21]. The results of these simulations are shown in Fig. 1, where the gold atomic fraction is given as function of depth;

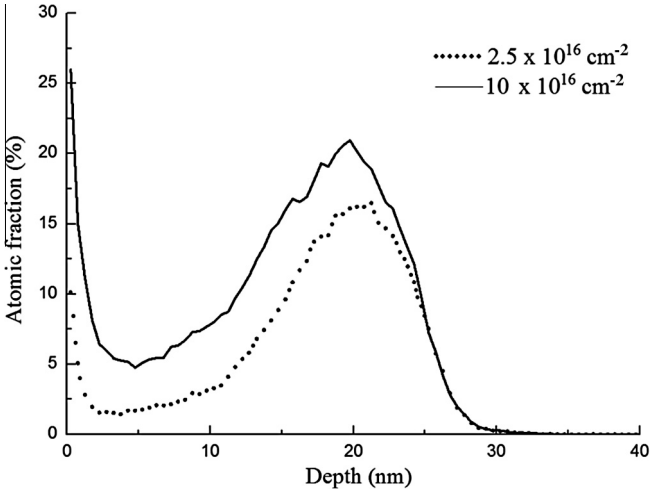

Fig. 1. TRIDYN simulations of the depth profiles for gold implanted into alumina with ion energy 40 keV and doses 2.5×10^{16} cm^{-2} and 10×10^{16} cm^{-2}. (We attribute the increase in concentration at shallow depth to an artifact of the program).

(the zero of depth is the alumina surface). We believe that the increase in gold concentration seen for shallow depth is an artifact of the program. The depth for the maximum gold atomic fraction for gold ions implanted into alumina with energy 40 keV is about 20 nm for doses 2.5×10^{16} cm^{-2} and 10×10^{16} cm^{-2}. It is known [35] that an excess of metal atom concentration above the solubility limit leads to nucleation and growth of metal nanoparticles, driven by the temperature and temperature gradients within the implanted sample including the beam-induced thermal characteristics. The gold nanoparticles nucleate near the maximum of the implantation depth profile [35], suggesting that the nanoparticles are buried 20 nm below the alumina surface.

The TEM results obtained here support the idea of gold nanoparticle formation. Au ion implantation was performed with ion energy of 40 keV and dose of 4.8×10^{16} cm^{-2}, and 32 TEM images were collected for the Au-implanted alumina. A typical TEM micrograph of the Au-implanted alumina is shown in Fig. 2, where one can see gold nanoparticles with average diameter of 3.2 nm.

For determining the saturation conductivity (σ_0) and the saturation dose (φ_0) for which the Au-implanted alumina still remains a composite, we calculated the normalized electrical conductivity, σ/σ_0, as a function of the normalized metal atom concentration, $x = \varphi/\varphi_0$, of the Au/alumina composite, using the Kirkpatrick equation given above. The calculated result is shown as the continuous curve in Fig. 3. The experimental results from two independent samples are also shown, where the saturation conductivity (σ_0) and the saturation dose (φ_0) have been adjusted so as to follow the theoretical curve (continuous line). The data points shown as squares and circles in the figure correspond to experimental results from these two independent samples, indicating the reproducibility of the results.

The saturation conductivity, σ_0, thus obtained for the Au/alumina composite was 14 S/m, which is about 10^4–10^5 times lower than the saturation conductivities for the Au/PMMA (2.0×10^6 S/m) and Pt/PMMA (0.5×10^6 S/m) composites, obtained by us in prior work [10–17]. The maximum dose φ_0 for which the Au/alumina system remains an insulator/conductor composite was found to be $\varphi_0 = 9.5 \times 10^{16}$ cm^{-2}, which is about 5 or 6 times the maximum dose of the Au/PMMA (2×10^{16} cm^{-2}) and Pt/PMMA (1.6×10^{16} cm^{-2}) composites. This result shows that although the maximum gold ion implantation dose is higher for the Au/alumina composite, its saturation conductivity σ_0 is much lower than the PMMA composites.

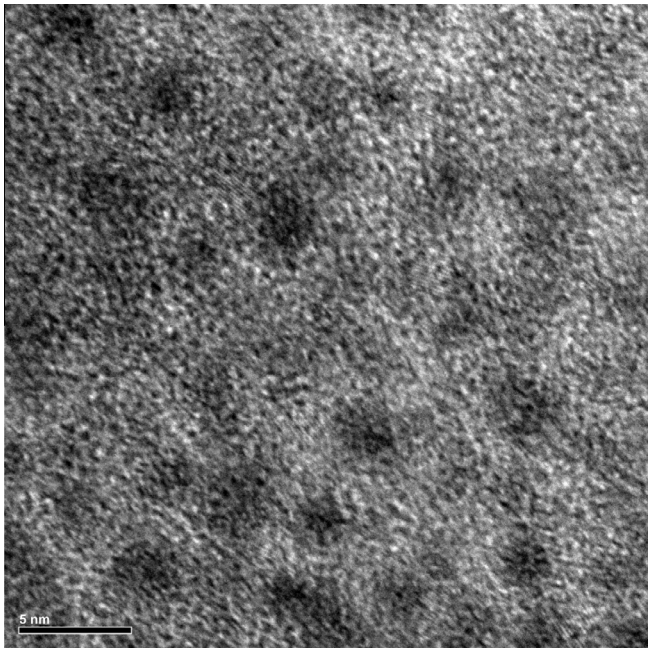

Fig. 2. TEM micrograph of Au-implanted alumina (ion energy 40 keV and dose 4.8×10^{16} cm^{-2}). The image shows gold nanoparticles with average diameter of 3.2 nm in the alumina matrix. The bar size is 5 nm.

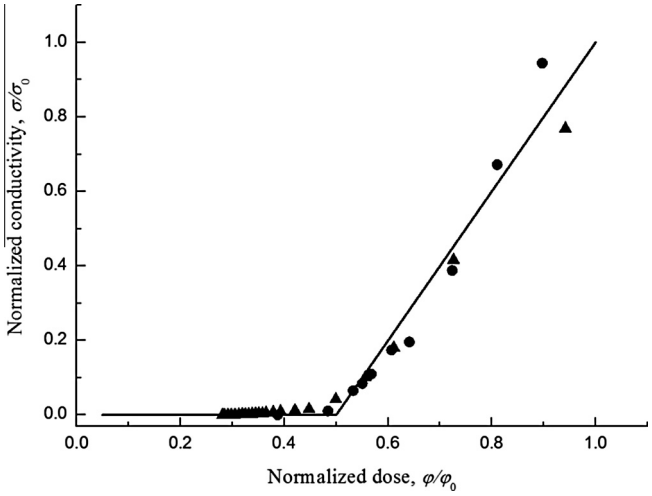

Fig. 3. Normalized electrical conductivity, σ/σ_0, as a function of normalized concentration of conducting phase, $x = \varphi/\varphi_0$, of the Au/alumina composite, using the Kirkpatrick equation (continuous line). The data points shown as squares and circles are experimental results from two independent samples, where the saturation conductivity (σ_0) and the saturation dose (φ_0) have been adjusted so as to follow the theoretical curve (continuous line).

The percolation dose φ_c for the Au/alumina composite was 4.4×10^{16} cm^{-2}, corresponding to $x_c = 0.46$, and the critical exponent obtained was $t = 1.4 \pm 0.1$. Since the critical exponent obeys the condition $t < 2.0$, we conclude that the conductivity process is due only to percolation and that the contribution from tunneling conduction is negligible [1].

Table 1 shows the percolation parameters and projected range for Au/PMMA [10–16], Pt/PMMA [15], Ti/alumina [18] and Au/alumina composites. It can be seen that although the absolute values of the saturation dose φ_0, saturation conductivity σ_0, and percolation dose φ_c are very different for PMMA and alumina composites, the normalized percolation dose $x_c = \varphi_c/\varphi_0$, the critical exponent t,

Table 1
Saturation dose φ_0, saturation conductivity σ_0, normalized percolation dose x_c, percolation dose φ_c, critical exponent t, and projected range Rp for Au/PMMA [10–16], Pt/PMMA [17], Ti/alumina [18] and Au/alumina (the present work) composites. The ion implantation energies were 49 eV for Au in PMMA, 67 eV for Pt in PMMA, 75 keV for Ti in alumina, and 40 keV for Au in alumina.

Composite	φ_0 (cm^{-2})	σ_0 (S/m)	$x_c = \varphi_c/\varphi_0$	φ_c (cm^{-2})	t	Rp (nm)
Au/PMMA	2×10^{16}	2.0×10^{6}	0.50	1×10^{16}	1.64	6.5
Pt/PMMA	1.6×10^{16}	0.5×10^{6}	0.31	0.5×10^{16}	1.46	7.0
Ti/alumina	10×10^{16}	50	0.4*	4×10^{16}	–	43
Au/alumina	9.5×10^{16}	14	0.46	4.4×10^{16}	1.4	20

*Estimated.

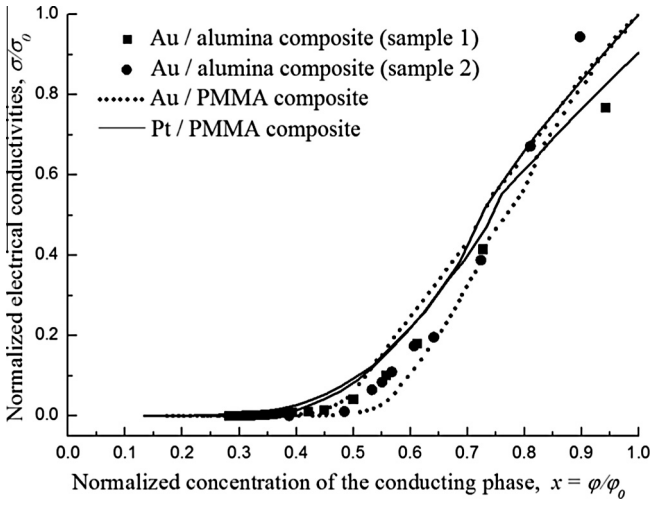

Fig. 4. Normalized electrical conductivity, σ/σ_0, as a function of normalized concentration of conducting phase, $x = \varphi/\varphi_0$, of the Au/alumina (this work), Au/PMMA [10–16], and Pt/PMMA [17] composites. Data from two independent experimental Au/alumina samples are shown, indicating the reproducibility of the results.

and the normalized electrical conductivity, σ/σ_0, as a function of the normalized metal atom concentration, $x = \varphi/\varphi_0$, are similar (see Fig. 4), as also observed for a vast class of disordered conducting-insulator compounds [1]. Note also that the saturation dose φ_0 and the percolation dose φ_c for Ti/alumina and Au/alumina composites are about 4–9 times greater than for Au/PMMA and Pt/PMMA composites. In addition, the saturation conductivity σ_0 for the alumina composites are about 10^4–10^5 times lower than for the PMMA composites. We thus conclude that, still having a percolated system, the alumina composites are much more resistive than the PMMA composites.

4. Conclusion

The surface electrical conductivity of gold-implanted alumina can be explained by a model in which an insulator-conductor composite of gold nanoparticles in alumina is formed in the implanted near-surface layer, and conductivity follows when the percolation process occurs. By considering the measured normalized electrical conductivity as a function of the normalized Au concentration of the conducting phase in the insulator-conductor composite, we have estimated the percolation parameters. For the 40 keV implantation energy used here, we estimate the percolation dose threshold to be about $\varphi_c = 4.4 \times 10^{16}$ cm^{-2}, and the saturation dose, i.e., the maximum dose for which the system remains an insulator-conductor composite, to be about $\varphi_0 = 9.5 \times 10^{16}$ cm^{-2}. The saturation electrical conductivity is estimated to be about 14 S/m. The mean diameter of the gold nanoparticle was found by TEM to be 3.2 nm (at an implantation dose of 4.8×10^{16} cm^{-2}).

Acknowledgments

This work was supported by the Fundação de Amparo a Pesquisa do Estado de São Paulo (FAPESP) and the Conselho Nacional de Desenvolvimento Científico e Tecnológico (CNPq), Brazil. We are grateful to the Institute of Ion Beam Physics and Materials Research at the Forschungszentrum Dresden-Rossendorf, Germany, for the TRIDYN-FZR computer simulation code.

References

[1] S. Vionnet-Menot, C. Grimaldi, T. Maeder, S. Strässler, P. Ryser, Phys. Rev. B 71 (2005) 064201.
[2] S. Kirkpatrick, Phys. Rev. Lett. 27 (1971) 1722.
[3] S. Kirkpatrick, Rev. Mod. Phys. 45 (1973) 574.
[4] C.W. White, C.J. McHargue, P.S. Sklad, L.A. Boatner, G.C. Farlow, Mater. Sci. Reports 4 (1989) 41.
[5] S. Anders, A. Anders, I. Brown, IEEE 1993 Particle Accelerator Conference, in: C.W. Leemann, J.J. Bisognano (Eds.), Pub IEEE 1994, Washington, D.C., May 17–20, (1993) (ISBN-0780312031).
[6] F. Liu, I. Brown, L. Phillips, G. Biallas, T. Siggins, IEEE Particle Accelerator Conference, Vancouver, B.C. Canada, May, 1997. 12–16.
[7] F. Liu, M.R. Dickinson, R.A. MacGill, A. Anders, O.R. Monteiro, I.G. Brown, L. Phillips, G. Biallis, T. Siggins, in: Surf. Coat. Technol. 103/104 (1998) 46.
[8] D. Li, J. Zhang, M. Yu, J. Kang, W. Li, Appl. Surf. Sci. 252 (2005) 1029.
[9] A. Nikolaev, E.M. Oks, K. Savkin, G.Yu. Yushkov, D.J. Brenner, G. Johnson, G. Randers-Pehrson, I.G. Brown, R.A. MacGill, Surf. Coat. Technol. 201 (2007) 8120.
[10] M.C. Salvadori, M. Cattani, F.S. Teixeira, I.G. Brown, Appl. Phys. Lett. 93 (2008) 073102.
[11] F.S. Teixeira, M.C. Salvadori, M. Cattani, I.G. Brown, J. Appl. Phys. 105 (2009) 064313.
[12] F.S. Teixeira, M.C. Salvadori, M. Cattani, S.M. Carneiro, I.G. Brown, J. Vac. Sci. Tech. B 27 (2009) 2242.
[13] F.S. Teixeira, M.C. Salvadori, M. Cattani, I.G. Brown, J. Vac. Sci. Tech. A 28 (2010) 818.
[14] F.S. Teixeira, M.C. Salvadori, M. Cattani, I.G. Brown, J. Appl. Phys. 106 (2009) 056106.
[15] F.S. Teixeira, M.C. Salvadori, M. Cattani, I.G. Brown, J. Appl. Phys. 108 (2010) 093505.
[16] F.S. Teixeira, M.C. Salvadori, M. Cattani, I.G. Brown, J. Appl. Phys. 111 (2012) 104311.
[17] M.C. Salvadori, F.S. Teixeira, M. Cattani, I.G. Brown, J. Appl. Phys. 110 (2011) 114905.
[18] M.C. Salvadori, F.S. Teixeira, M. Cattani, A. Nikolaev, K.P. Savkin, E.M. Oks, H.-K. Park, L. Phillips, K.M. Yu, I.G. Brown, J. Appl. Phys. 111 (2012) 063714.
[19] M.C. Salvadori, F.S. Teixeira, W.W.R. Araújo, L.G. Sgubin, R.E. Spirin, M. Cattani, I.G. Brown, J. Appl. Phys. 112 (2012) 074312.
[20] W. Möller, W. Eckstein, Nucl. Instr. Meth. Phys. Res. B 2 (1984) 814.
[21] W. Möller, W. Eckstein, J.P. Biersack, Comput. Phys. Commun. 51 (1988) 355.
[22] I.G. Brown, M.R. Dickinson, J.E. Galvin, X. Godechot, R.A. MacGill, Nucl. Instr. Meth. B 55 (1991) 506.
[23] I. Brown, E. Oks, IEEE Trans. Plasma Sci. 33 (6) (2005) 1931.
[24] I.G. Brown, A.G. Nikolaev, R.A. MacGill, E.M. Oks, K.P. Savkin, G.Yu. Yushkov, Izv. Vyssh. Uchebn. Zaved. Fiz. 8 (2006) 5.
[25] I.G. Brown, Vacuum Arc Ion Sources, The Physics and Technology of Ion Sources, Ian Brown, E.M. Oks, I.G. Brown (Eds.), Wiley, New York, (1994); Vacuum Arc Ion Sources, The Physics and Technology of Ion Sources, 2nd ed., Ian Brown (Ed.), Wiley-VCH, Weinheim, (2004).
[26] M.C. Salvadori, F.S. Teixeira, L.G. Sgubin, W.W.R. Araujo, R.E. Spirin, E.M. Oks, K.M. Yu, I.G. Brown, Appl. Phys. Lett. 101 (2012) 224104.
[27] R.L. Boxman, D.M. Sanders, P.J. Martin (Eds.), Handbook of Vacuum Arc Science & Technology, Noyes, Park Ridge, N.J., 1995.
[28] A. Anders, Cathodic Arcs: From Fractal Spots to Energetic Condensation, Springer, New York, 2008.
[29] I.G. Brown, Cathodic arc deposition of films, Annu. Rev. Mater. Sci. 28 (1998) 243.

[30] D.R. Martins, M.C. Salvadori, P. Verdonck, I.G. Brown, Appl. Phys. Lett. 81 (2002) 1969.
[31] M.C. Salvadori, L.L. Melo, A.R. Vaz, R.S. Wiederkehr, F.S. Teixeira, M. Cattani, Surf. Coat. Technol. 200 (2006) 2965.
[32] I.G. Brown, X. Godechot, IEEE Trans. Plasma Sci. 19 (1991) 713.
[33] I. Brown, E. Oks, IEEE Trans. Plasma Sci. 33 (2005) 1931.
[34] J.F. Ziegler, J.P. Biersack, U. Littmark, The Stopping and Range of Ions in Solids Pergamon, New York, (1985) (new edition in 1996). The computer code is downloadable from the SRIM website <http://www.srim.org/>.
[35] A.L. Stepanov, D.E. Hole, P.D. Townsend, J. Non-Crystalline Solids 260 (1999) 65.